IEEE Photonics Journal
An IEEE Photonics Society Publication

Open Access

Optical Fiber Tip Sensor for the Measurement of Glucose Aqueous Solutions

Volume 10, Number 5, September 2018

Susana Novais
Catarina I. A. Ferreira
Marta S. Ferreira
João L. Pinto

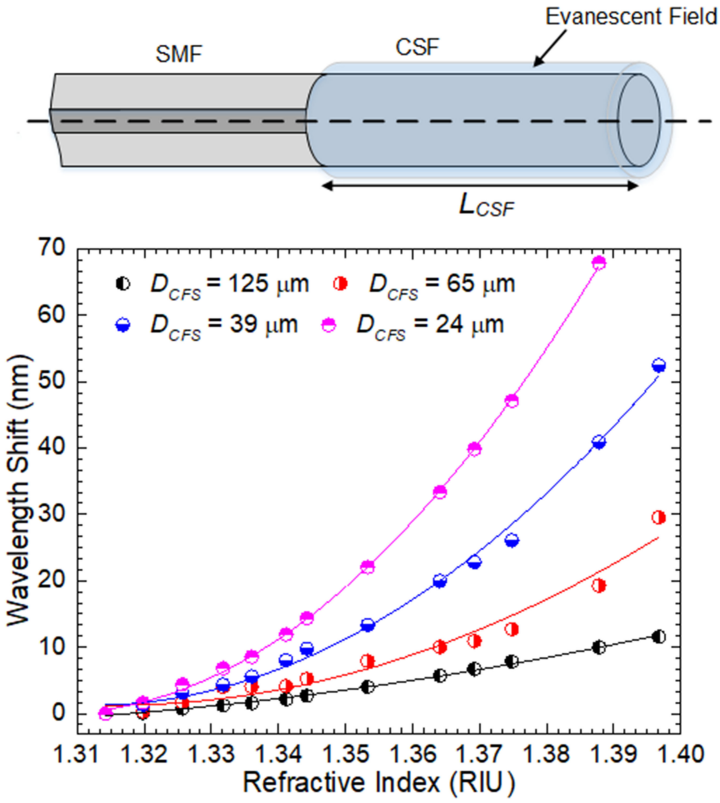

DOI: 10.1109/JPHOT.2018.2869944
1943-0655

IEEE photonics SOCIETY

IEEE

Optical Fiber Tip Sensor for the Measurement of Glucose Aqueous Solutions

Susana Novais, Catarina I. A. Ferreira, Marta S. Ferreira, and João L. Pinto

I3N & Department of Physics, University of Aveiro, Campus de Santiago, Aveiro 3810-193, Portugal

DOI:10.1109/JPHOT.2018.2869944

Manuscript received June 15, 2018; revised September 6, 2018; accepted September 9, 2018. Date of publication September 13, 2018; date of current version September 26, 2018. This work was supported in part by FEDER funds through the COMPETE 2020 Programme and in part by National Funds through FCT-Portuguese Foundation for Science and Technology under the Project UID/CTM/50025/2013 and POCI-01-0145-FEDER-016414. The work of Susana Novais, Catarina I. A. Ferreira, and Marta S. Ferreira was supported by research fellowships BI/UI96/6643/2016, SATCTPAC1003612015, BPD/UI96/6274/2017, and SFRH/BPD/124549/2016, respectively. Corresponding author: Susana Novais (e-mail: novais@ua.pt).

Abstract: A reflective fiber optic sensor based on multimode interference for the measurement of refractive index variations in glucose aqueous solutions is proposed. The sensor is fabricated by splicing a short section of coreless silica fiber to standard single mode fiber. The influence of the coreless fiber dimensions on the sensor performance is analyzed. By changing the sensor length, no significant impact is observed. However, the reduction of the sensing head diameter leads to a large improvement of the sensitivity. The smaller sensor, with a length of 5 mm and a diameter of 24 μm, presents a maximum sensitivity of 1467.59 nm/RIU, for the refractive index range between 1.364 and 1.397 RIU. Taking into account the acquisition system, a maximum theoretical resolution of 6.8×10^{-5} RIU is achieved.

Index Terms: Fiber optic sensors, multimode interferometry, refractive index sensing, chemical analysis.

1. Introduction

The multimode interference (MMI), as typically example the single mode-multimode-single mode (SMS) structure, has been explored as an attractive technology on optical communications and sensing. Due to the clear advantages of simplicity, low-cost, facility of manufacture, and high repeatability, it emerges as an alternative to existing fiber-based refractometers [1], or for strain measurement with temperature compensation [2], curvature sensing [3] or in edge filtering for wavelength measurement [4]. The subjacent operating principle of this kind of sensors is the MMI excited between modes in the multimode fiber (MMF) section, which can be influenced by external perturbations [5], [6]. To perform refractive index sensing based on the SMS fiber structure, different techniques have been reported. For instance, a MMF core section was sandwiched between two single mode fibers (SMFs), where the MMF cladding was removed through chemical etching [1]. Zhao *et al*. proposed a sensor composed by two sections of SMF and one section MMF, with high sensitivity to refractive index [7]. Jung *et al*. reported a compact surrounding refractive-index sensor

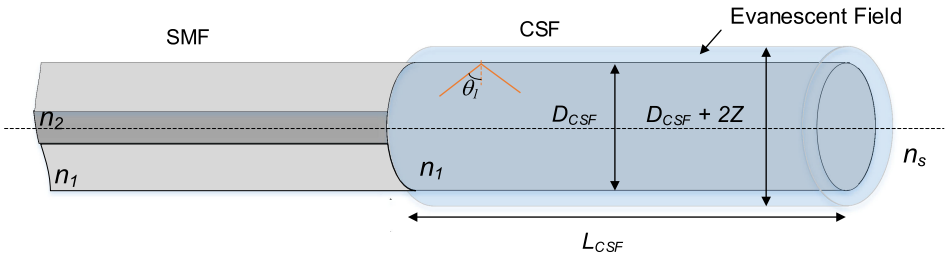

Fig. 1. Schematic diagram of the sensor structure, where n_1 is both the refractive index of the SMF cladding and the coreless fiber, n_2 and n_s are the refractive index of SMF core and surrounding medium; L_{CSF} and D_{CSF} are the coreless fiber length and diameter, respectively, and Z is the evanescent field penetration depth.

using a multimode-coreless-multimode structure [8]. A SMS fiber structure used in combination with a uniform Bragg grating [9] and an enhanced evanescent field fiber sensor based on a tapered MMF sandwiched between two SMFs [10] have also been reported for refractive index measurement. Regarding the use of a coreless silica fiber as sensing device, some works have also been reported for the measurement of refractive index [11] and temperature [12], however the measurements were usually based on a transmission scheme [13], [14].

In many fields such as disease diagnosis, clinical analysis and quality monitor in food industry, the rapid and precise detection of glucose concentration is vital. In particular, the abnormal body blood glucose level monitoring is critically essential for human health [15]. The significance of glucose detection and potential commercial value has attracted constant effort on research. One of the used key methods for glucose sensing is centered on fluorescently labeled sensing schemes, which employ changes in fluorescent intensity to reflect sample concentration [16], but the short lifetime of fluorescent agents and the high cost of enzymes limit their further development and application in biosensing [17]. For that reason, the development of low-cost and robust sensing methods is highly desirable. A surface plasmon resonance fiber sensor based on a multimode plastic clad silica fiber was coated with silver and silicon films. Glucose oxidase was immobilized at the fiber surface for the detection of low levels of glucose [18]. A long period fiber grating coated with enzyme was firstly proposed by Deep *et al*. for the measurement of glucose. A linear relationship was found in the range of 10–300 mg dL^{-1} [19]. The same immobilization technique was used on a fiber with an 81° tilted Bragg grating (TFBG). A low temperature cross-talk, good linearity and Q-factor was achieved in the proposed glucose sensor [20]. A glucose sensor based on enzymatic graphene oxide functionalized TFBG was also proposed. The analytical range considered was of 0–8 mM, which contains the biological region for human blood glucose levels [21].

In this work, a multimode fiber tip interferometer based on an etched coreless silica fiber is proposed for the measurement of the refractive index variations of glucose aqueous solutions. A comparison between the performance of sensors with similar diameters and different lengths, and similar lengths and different diameters is performed.

The reflection configuration has several advantages over the inline MMIs. On one hand, the length is reduced by half, since light is reflected at the coreless end face and recoupled to the single mode fiber. On the other hand, the cleaning procedure is easier, smaller amounts of analyte can be employed, the sensing structure becomes less fragile, even after etching, and it can be placed at a long distance regarding the acquisition system, thus becoming a good alternative in harsh environments where refractive index or concentration variations need to be monitored.

2. Sensor and Operation Principle

The sensing device developed in this work consists on a short section of coreless silica fiber (CSF) spliced to single mode fiber (SMF), as shown in Fig. 1. Light is guided through the SMF and when it enters the coreless fiber section, several modes are excited and guided until the fiber end section

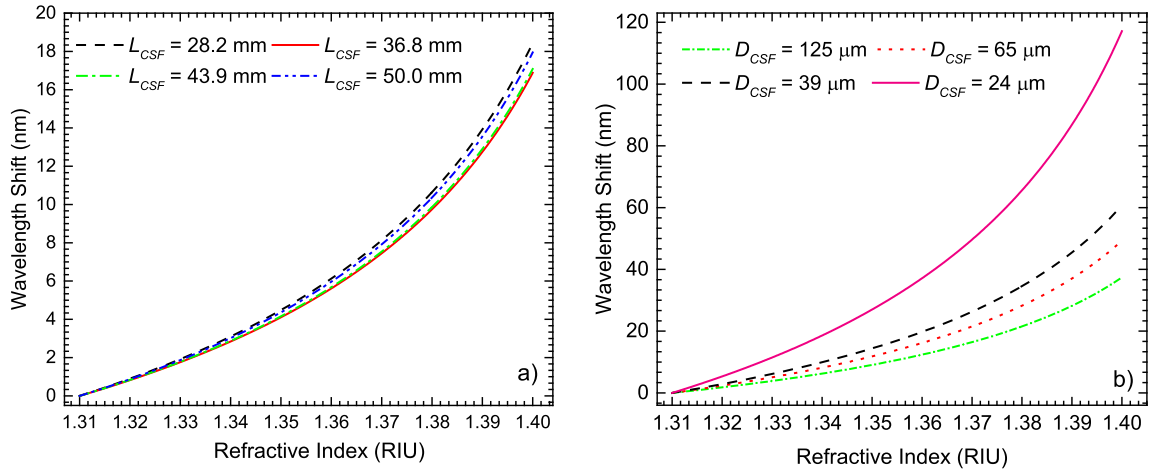

Fig. 2. Simulated wavelength shift dependence on external media refractive index, considering (a) constant diameter and different lengths and (b) constant length and different diameters.

is achieved. Due to the Fresnel reflection, a small fraction of the light is reflected and recoupled once again to the SMF fundamental mode.

The interference wavelength, λ_0, can be expressed according to Eq. 1 [22]:

$$\lambda_0 = \frac{n_1 D_{CSF}^2}{2L_{CSF}} p, \tag{1}$$

where n_1, D_{CSF}, and L_{CSF} are the CSF refractive index, diameter, and length, respectively, whereas p is the interference number. One of the important characteristics of a multimode interferometer (MMI), is that λ_0 can be easily designed to be in the wavelength region used, by selecting the appropriate dimensions [22]. When $p = 4$, the self-image is formed due to the constructive interference between several guided modes, and the sensor presents lowest losses [13]. However, at different interference numbers, even though no self-image is present, the constructive interference between two consecutive modes with high coupling efficiency can originate a spectrum that, although with higher losses, is still suitable to perform measurements.

From Equation 1, there is no obvious dependence of the wavelength with the external medium. However, if one considers the evanescent field generated at the CSF/external media interface, the diameter can be considered as an effective value of $D + 2Z$, where Z corresponds to the penetration depth. This parameter is given by Eq. 2 [12],

$$Z = \frac{\lambda_0}{2\pi n_1 \sqrt{\sin^2\theta - (n_s/n_1)^2}}, \tag{2}$$

where n_s is the surrounding medium refractive index and θ is the incident angle at the CSF/surrounding medium interface, as shown in Fig. 1. As the environmental refractive index changes, the propagation constants for each guided mode within the CSF will change too, which leads to shifts in the output spectra, owing to the direct exposure of the CSF [23].

To determine the influence of both CSF length and diameter on the sensitivity of the developed sensors, the previous equations were combined and solved in order to obtain the wavelength dependence on refractive index. The CSF refractive index was considered to be 1.444 at 1550 nm, and θ was estimated to be 84.94° [24]. In the first part of the simulation, the diameter was fixed to be 125 μm, and the length varied between 28.2 mm and 50.0 mm (Fig. 2(a)). In the second part, the length parameter was kept constant (5 mm), and the diameter was changed between 125 μm and 24 μm (Fig. 2(b)). The interference order p was estimated using Equation (1), for an operation wavelength within the 1550 nm range.

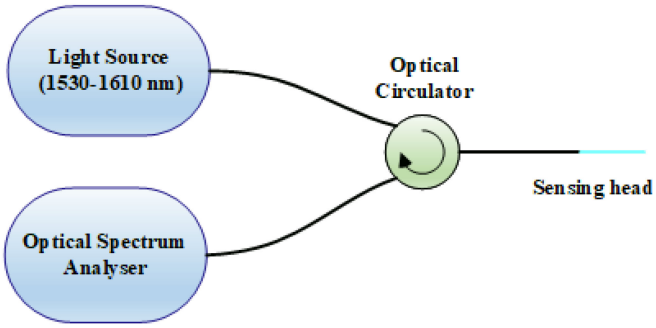

Fig. 3. Scheme of the experimental setup.

As can been seen in the simulation results, the wavelength shift increases non-linearly with the surrounding refractive index. This behavior is expected until the refractive index of the external medium becomes close to the one of the CSF. In this case, the total internal reflection condition ceases to exist, and no light is expected to be reflected at in the sensor region. In Fig. 2(a), there is no direct correlation between the CSF length and the wavelength shift. However, if the ratio between L_{CSF} and p is taken into account, the relationship becomes clearer: larger values of L_{CSF}/p lead to lower sensitivities. For instance, a 36.8 mm long sensor ($L_{CSF}/p = 7.36$) has a similar response to the one with a length of 43.9 mm ($L_{CSF}/p = 7.32$), whereas the sensors with lengths of 50.0 mm ($L_{CSF}/p = 7.14$) and 28.2 mm ($L_{CSF}/p = 7.05$) are more sensitive than in the previous cases. This ratio can be used to maximize the sensors sensitivity, according to the desired application. Nevertheless, in this case no significant changes are observed in the sensors response, meaning that the variation of length does not play a decisive role in the sensitivity. However, the smaller the diameter, the more significant becomes the evanescent field, which translates into higher sensitivities.

3. Results

Figure 3 presents the scheme of the experimental setup used in this work, both for the refractive index measurements in liquid media and for the temperature experiments. The sensing structure spectral response was observed in a typical reflection scheme, by connecting the broadband optical source (bandwidth of 80 nm, centered at 1570 nm), the sensing head, and the optical spectrum analyzer (OSA Anritsu MS9740A) to the three ports of an optical circulator. The readings were performed with a resolution of 0.1 nm.

A series of glucose aqueous solutions were prepared under a controlled laboratory environment, with glucose mass fractions ranging from 0 wt.% to ~45 wt.%. A magnetic stirrer (NAHITA, magnetic stirred, model n° 690/1) was used to dilute the glucose in the deionized water. After the preparation, the samples were stored for 24 hours, to allow their stabilization. The refractive index experiments were carried out at room temperature (~23 °C), under a controlled environment. The sensor was inserted vertically in the different solutions with the aid of capillary glass tube. However, the sensing area was kept outside this tube, in direct contact with the measurand. This setup ensured the sensor robustness as well as the stability of the fiber inside the liquid.

Figure 4 presents the shifts in the reflection spectra due to the direct exposure of the CSF under different percentages of glucose, for one sensing head with a diameter of 125 μm and a length of 59.6 μm (sensor 1). With the increase of the mass fraction, not only the amplitude of the reflected spectra changes, but there is also a notorious wavelength shift. This is related to the increase of the solutions refractive index with the increase of glucose concentration in the aqueous solution.

The refractive index of each solution was measured using an Abbe refractometer (Krüss optronic refractometer), that provides information in the spectral visible range ($\lambda = 589$ nm). Since the optical source used in the experiments was centered in the 1550 nm region, it was necessary to first calibrate the solutions and thus estimate the refractive index at this wavelength range.

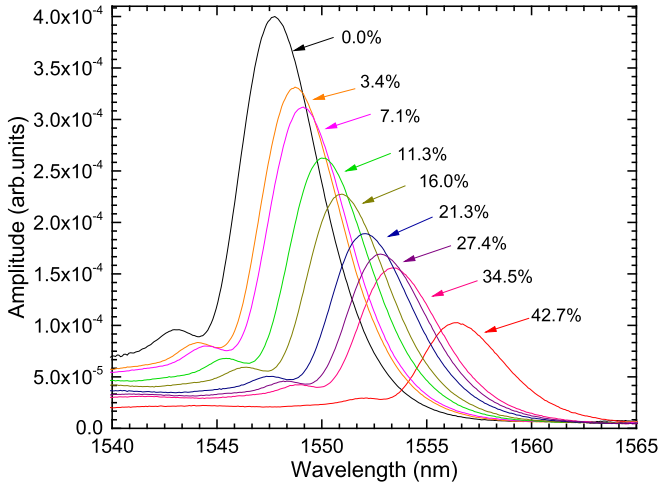

Fig. 4. Output spectra of sensor 1 under different mass fraction percentages of glucose.

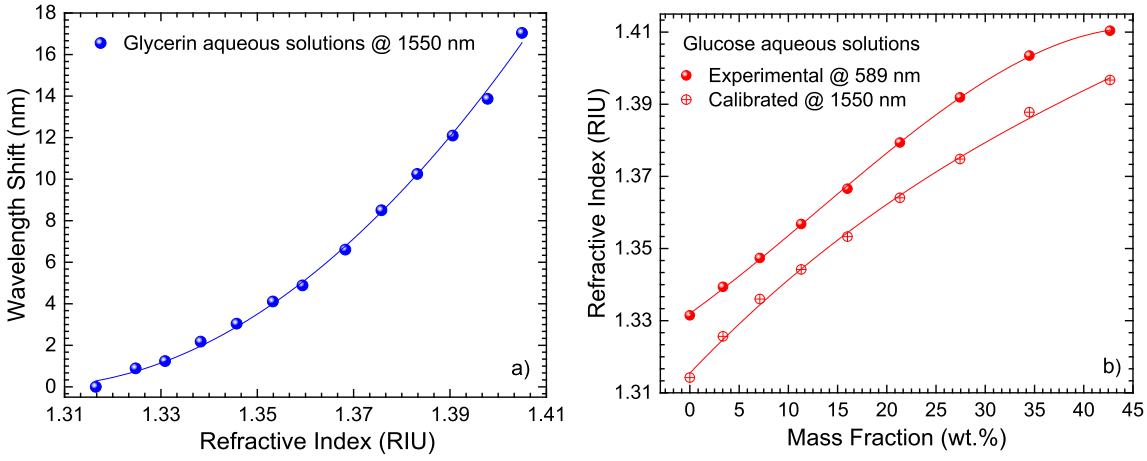

Fig. 5. Sensor calibration to refractive index measurements. (a) wavelength shift dependence on refractive index of glycerin aqueous solutions, for an operating wavelength of 1550 nm and (b) refractive index variation with mass fraction for glucose aqueous solutions, at 589 nm, measured through the Abbe refractometer and 1550 nm, determined from the calibration.

This was achieved by subjecting sensor 1 to previously calibrated glycerin aqueous solutions, where the refractive index at 1550 nm has been determined [25]. The wavelength shift ($\Delta\lambda$) dependence on refractive index (n), shown in Fig. 5(a), was adjusted by the second order polynomial (Eq. 3):

$$\Delta\lambda = 2725.11 - 4181.72n + 1604.23n^2, \tag{3}$$

with a correlation factor of 0.998. The same sensor was then evaluated for each glucose-water mixture and, by using the previous equation, it was possible to convert wavelength variations into refractive index. Fig. 5(b) shows the relation between refractive index and mass fraction for the glucose solutions at the two wavelength regions considered. It is possible to observe that in both cases the behavior is similar. A third-order polynomial fit was applied to the data, according to Eq. 4:

$$n(w) = A + Bw + Cw^2 + Dw^3, \tag{4}$$

where w indicates the solubility range as weight fraction, whereas A, B, C, and D are the fitting parameters. The values are gathered in Table 1.

TABLE 1
Parameters for Third Order Polynomial Fits of the Refractive Index Dependence on Mass Fraction for Glucose Solutions, at 589 nm and 1550 nm

	Glucose (1550 nm)	Glucose (589 nm)
w	0 - 0.45	0 - 0.45
A	0.1686	-7.1865×10^{-7}
B	-0.2796	2.8140×10^{-5}
C	0.2778	0.0019
D	1.3166	1.3320

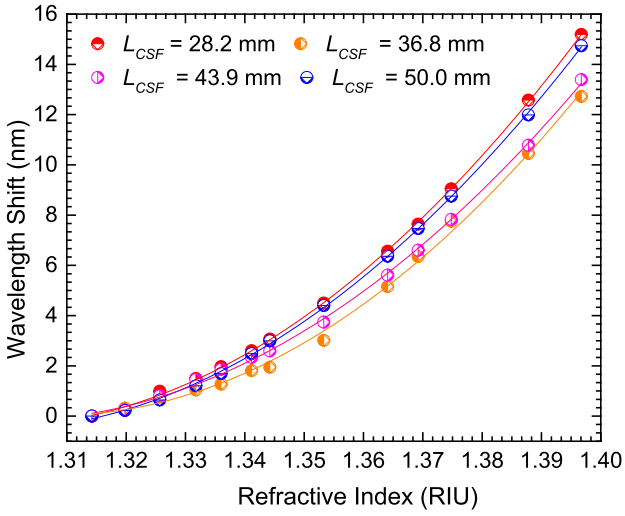

Fig. 6. Sensors response to refractive index variations for sensors with different lengths.

TABLE 2
Sensitivities Obtained for Each Sensor

Sensor characteristics			1.316 – 1.353		1.364 – 1.397	
p	D_{CSF} **(μm)**	L_{CSF} **(mm)**	k_n **(nm/RIU)**	r^2	k_n **(nm/RIU)**	r^2
4	125	28.2	114.42	0.976	266.53	0.997
5		36.8	73.49	0.971	228.68	0.998
6		43.9	96.49	0.989	236.93	0.994
7		50.0	113.29	0.952	255.44	0.995

Four sensors with lengths ranging from 28.2 mm to 50.0 mm were fabricated. Considering the refractive index of the CSF to be 1.444, and the operation wavelength in air of ~1530 nm, p was estimated to be between 4 and 7. Although the self-image occurs at $p = 4$, and lower losses are obtained, the sensors revealed to be adequate to perform refractive index measurements. The results are shown in Fig. 6. As expected, in all cases the behavior is non-linear, following the tendency described in Section 2. Furthermore, it is observed that there are no significant changes regarding the sensor sensitivity. Two different linear regions were considered to estimate the sensors sensitivity, k_n. The first region, for lower refractive index variations, ranges from 1.316 RIU and 1.353 RIU, whereas the higher refractive index variations were considered between 1.364 RIU and 1.397 RIU. The sensitivities attained are shown in Table 2 , where D_{CSF} and L_{CSF} are the CSF diameter and length, respectively.

TABLE 3
Sensitivities Obtained for Each Sensor

	Sensor characteristics		1.316 – 1.353		1.364 – 1.397	
p	L_{CSF} (mm)	D_{CSF} (μm)	k_n (nm/RIU)	r^2	k_n (nm/RIU)	r^2
1	5	125	102.42	0.959	177.69	0.999
3		65	197.84	0.903	582.54	0.945
7		39	338.23	0.972	1012.66	0.974
19		24	544.88	0.956	1467.59	0.995

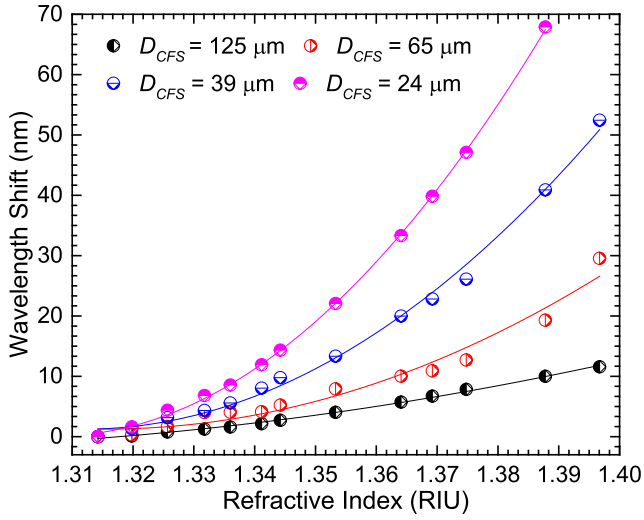

Fig. 7. Sensors response to refractive index variations.

The length of the sensing device can be a limiting factor in practical applications. When using sensors with several centimeters in length, not only the sensors become more fragile, but also larger sampling volumes are required, since the liquid must be in contact with the whole sensing structure. However, in order to have a reflection spectrum with a peak in the 1550 nm region, and considering smaller lengths, it is necessary to reduce the fiber diameter as well. Besides, as it was observed in Section 2, an increase of the sensor sensitivity is expected with the decrease of the diameter. To further test the sensing performance and evaluate the practicability of these sensors, four different samples with a length of ∼5 mm were produced. Three of these sensors were subjected to wet chemical etching using a 40% hydrofluoric acid (HF) solution. To obtain a structure with a nearly constant core diameter over its length, as well as a smooth surface, the HF solution was placed inside an ultrasound bath at room temperature.

A preliminary experiment was performed to determine the etching rate. A sample of CSF was submerged in liquid HF, at room temperature, for a few minutes, after which it was removed from the solution and cleaned thoroughly with ethanol. A microscope picture was taken to estimate the CSF diameter. The sample was once one again placed in the etching solution for a few additional minutes and the process was repeated. An etching rate of 1.63 μm/min was determined.

Figure 7 presents the wavelength dependence with the refractive index variations for the sensors with different CSF diameters, which ranged from 125 μm to 24 μm, translating into p values between 1 and 19. As observed for the non-etched sensors, a non-linear response is obtained. However, in this case, the difference between each sensor response is more significant and, as expected, the sensor with a smallest diameter presented the highest sensitivity. Once again, two different ranges can be considered, between 1.316 RIU and 1.353 RIU, and between 1.364 RIU and 1.397 RIU. Table 2 summarizes the sensitivities to refractive index (k_n) obtained for each sensor, in both regions

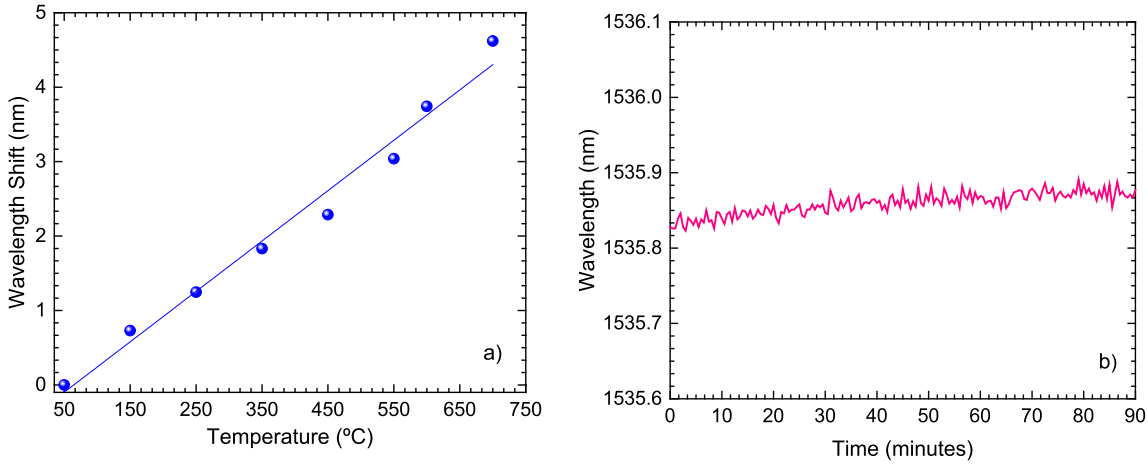

Fig. 8. Response of the sensor with a diameter of 125 μm to temperature variations (a) and long term stability experiment, using a solution of water at room temperature (b).

considered. As can be seen from the results, as the diameter of the CSF decreases, the sensitivity increases, in both ranges presented. The thinnest sensor is 8.3$\times$ more sensitive than the one with largest diameter, for the higher refractive index range. Considering the sensor with the highest sensitivity and the OSA resolution, a maximum theoretical resolution of 6.8×10^{-5} RIU is achieved [26]. The results indicate that it is possible to tailor the sensor dimensions according to the desired sensitivity and to the application. Larger sensors, on one hand, do not exhibit high sensitivities, and require higher volume samples. On the other hand, smaller sensors present better responses. However, as the diameter decreases, the fiber becomes more fragile. In such case, and considering a practical application, a suitable package should be developed to ensure robustness of the sensor. Nevertheless, in all cases the sensors presented a fast response and were very stable in the liquid media.

The temperature response was measured by placing the sensor with a diameter of 125 μm and with a length of 43.9 mm, in a tubular oven with a resolution of 1 °C. The temperature was increased in steps of 100 °C, until 700 °C, and maintained for about 20 min at each step to make sure that the temperature in the oven had stabilized. Fig. 8(a) presents the sensor response towards this parameter. It exhibited thermal dependence of 6.8 pm/°C, with a correlation factor of 0.978. The sensitivity towards temperature is essentially due to the silica thermal expansion, being comparable to that of a fiber Bragg grating [27]. The sensor stability was evaluated by placing the sensor in the water solution, at room temperature, for 90 minutes. The spectrum was acquired every 30 seconds. The peak wavelength variations with time, is shown in Fig. 8(b). The mean value was of 1535.86 nm and the standard deviation was of 0.01 nm. During the experiment, the temperature fluctuations were of 0.2 °C. The proposed sensor revealed high stability, the results are reproducible, and the cross-sensitivity was determined to be 7.1×10^{-5} RIU/°C.

4. Conclusion

In summary, a high-sensitivity reflective optical fiber sensor based on coreless silica fiber for the measurement of refractive index variations in glucose aqueous solutions was proposed. The sensor was fabricated by splicing standard single mode fiber to a short section of coreless silica fiber (CSF). Firstly, four sensors with the same diameter and different lengths were used to perform refractive index measurements. It was observed that the CSF length has no significant influence on the sensitivity to external medium variations. The influence of the sensor diameter was studied by using four samples with similar lengths. Three of such samples were subjected to wet chemical etching using a 40% hydrofluoric acid solution, to decrease their diameter. It was observed that as

the diameter decreased, the sensitivity increased significantly. In fact, the sensor with the smaller diameter presented a maximum sensitivity of 1467.59 nm/RIU, for the refractive index range between 1.364 RIU and 1.397 RIU. By reducing the structure diameter, an enhancement of $\sim$8.3$\times$ was achieved. In practical applications, the sensitivity to temperature should be compensated with a suitable method. The developed structure has attractive advantages, such as simple structure, fast response and stability. It has possibilities to expand in various sensing applications, where the use of only a fiber tip can be a better alternative to inline multimode interference sensors.

References

[1] Q. Wang and G. Farrell, "All-fiber multimode-interference-based refractometer sensor: Proposal and design," *Opt. Lett.*, vol. 31, pp. 317–319, 2006.
[2] A. M. Hatta, Y. Semenova, Q. Wu, and G. Farrell, "Strain sensor based on a pair of single-mode-multimode-single-mode fiber structures in a radiometric power measurement scheme," *Appl. Opt.*, vol. 49, pp. 536–541, 2010.
[3] S. Silva *et al.*, "Temperature and strain independent curvature sensor based on a singlemode/multimode fiber optic structure," *Meas. Sci. Technol.*, vol. 22, 2011, Art. no. 085201.
[4] Q. Wang and G. Farrell, "Multimode-fiber-based edge filter for optical wavelength measurement application and its design," *Microw. Opt. Technol. Lett.*, vol. 48, pp. 900–902, 2006.
[5] L. B. Soldano and E. C. M. Penning, "Optical multi-mode interference devices based on self-imaging: principles and applications," *J. Lightw. Technol.*, vol. 13, no. 4, pp. 615–627, Apr. 1995.
[6] X. Zhou, K. Chen, X. Mao, W. Peng, and Q. Yu, "A reflective fiber-optic refractive index sensor based on multimode interference in a coreless silica fiber," *Opt. Commun.*, vol. 340, pp. 50–55, 2015.
[7] Y. Zhao, L. Cai, and X. L. Z Zhao, "Investigation of the high sensitivity RI sensor based on SMS fiber structure," *Sens. Actuators, A.*, vol. 205, pp. 186–190, 2014.
[8] Y. Jung, S. Kim, D. Lee, and K. Oh, "Compact three segmented multimode fibre modal interferometer for high sensitivity refractive-index measurement," *Meas. Sci. Technol.*, vol. 17, pp. 1129–1133, 2006.
[9] Q. Wu, Y. Semenova, P. Wang, and G. Farrel, "High sensitivity SMS fiber structure based refractometer-analysis and experiment," *Opt. Exp.*, vol. 19, pp. 7937–7944, 2011.
[10] P. Wang, G. Brambilla, M. Ding, Y. Semenova, and Q. Wu, "A high sensitivity, evanescent field refractometric sensor based on tapered multimode fiber interference," *Opt. Lett.*, vol. 36, pp. 2233–2235, 2011.
[11] I. Del Villar, A. B. Socorro, J. M. Corres, F. J. Arregui, and I. R. Matias, "Refractometric sensors based on multimode interference in a thin-film coated singlemode–multimode–single-mode structure with reflection configuration," *Appl. Opt.*, vol. 53, pp. 3913–3919, 2014.
[12] H. Fukano, Y. Kushida, and S. Taue, "Sensitivity improvement of optical-fiber temperature sensor with solid cladding material based on multimode interference," *Jap. J. Appl. Phys.*, vol. 54, 2015, Art. no. 032502.
[13] S. Silva *et al.*, "Ultrahigh-sensitivity temperature fiber sensor based on multimode interference," *Appl. Opt.*, vol. 51, pp. 3236–3242, 2012.
[14] H. Fukano, Y. Kushida, and S. Taue, "Multimode-interference structure optical-fiber temperature sensor with high sensitivity," *Elect. Exp.* vol. 10, pp. 1–5, 2013.
[15] Y. Li *et al.*, "Immobilized optical fiber microprobe for selective and high sensitive glucose detection," *Sens. Actuators, B*, vol. 255, pp. 3004–3010, 2018.
[16] R. Ballerstadt, A. Polak, A. Beuhler, and J. Frye, "In vitro long-term performance study of a near-infrared fluorescence affinity sensor for glucose monitoring," *Biosens. Bioelectron.*, vol. 19, pp. 905–914, 2004.
[17] R. Esposito *et al.*, "Glucose sensing by time-resolved fluorescence of sol–gel immobilized glucose oxidase," *Sensors.*, vol. 11, pp. 3483–3497, 2011.
[18] S. Sarika and D. Banshi, "Fabrication and characterization of a surface plasmon resonance based fiber optic sensor using gel entrapment technique for the detection of low glucose concentration," *Sens. Actuators, B.*, vol. 177, pp. 589–595, 2013.
[19] A. Deep *et al.*, "Immobilization of enzyme on long period grating fibers for sensitive glucose detection," *Biosens. Bioelectron.*, vol. 33, pp. 190–195, 2012.
[20] B. Luo, Z. Yan, Z. Sun, J. Li, and L. Zhang, "Novel glucose sensor based on enzyme-immobilized 81tilted fiber grating," *Opt. Exp.*, vol. 22, pp. 30571–30578, 2014.
[21] B. Jiang *et al.*, "Label-free glucose biosensor based on enzymatic graphene oxide-functionalized tilted fiber grating," *Sens. Actuators, B.*, vol. 254, pp. 1033–1039, 2017.
[22] J. E. Antonio-Lopez, A. Castillo-Guzman, D. A. May-Arrioja, R. Selvas-Aguilar, and P. LiKamWa, "Tunable multimode-interference bandpass fiber filter," *Opt. Lett.*, vol. 35, pp. 324–326, 2010.
[23] Y. Li, Z. Liu, and S. Jian, "Multimode interference refractive index sensor based on coreless fiber," *Photon. Sens.*, vol. 4, pp. 21–27, 2014.
[24] Y. Raichlin and A. Katzir, "Fiber-optic evanescent wave spectroscopy in the middle infrared," *Appl. Spectrosc.*, vol. 62, pp. 55A–72A, 2008.
[25] S. Novais, M. S. Ferreira, and J. L. Pinto, "Optical fiber Fabry–Perot tip sensor for detection of water–glycerin mixtures," *J. Lightw. Technol.*, vol. 36, pp. 1576–1582, May 2018.
[26] F. Chiavaioli, C. Gouveia, P. Jorge, and F. baldini, "Towards a uniform metrological assessment of grating-based optical fiber sensors: from refractometers to biosensors," *Biosensors.*, vol. 7, 2017, Art. no. e23.
[27] Y.-J. Rao, "In-fibre Bragg grating sensors," *Meas. Sci. Technol.*, vol. 8, pp. 355–375, 1997.